RESEARCH

Enhanced Photoelectric Responsivity of Graphene/GaAs Photodetector Using Surface Plasmon Resonance Based on Ellipse Wall Grating-Nanowire Structure

Yujiao Wang[1] · Yujuan Fu[1] · Jijie Zhao[1] · Huan Liu[1] · Lier Deng[1]

Abstract

High-efficiency integrated photodetectors can assist in future high-speed communication devices for achieving high responsivity characteristics. In this paper, we designed and optimized a graphene/GaAs heterojunction photodetector based on ellipse wall grating-nanowire (EWG-NW) structure. We evaluated the optical and electrical performance of the photodetector between 400 and 800 nm by COMSOL. Compared with graphene/GaAs heterojunction photodetector based on plain structure, our device exhibits enhanced responsivity performance within the visible spectrum at 0 bias voltage. The maximum photocurrent responsivity of 514 mA/W (increased by 56%) and detectivity of 1.16×10^{11} Jones (increased by 41%) are achieved at 725 nm. The mechanism of improvement originates from surface plasmon resonance-enhanced electromagnetic field excited by elliptical wall gratings and metal nanowires in graphene/GaAs heterostructures, thus significantly enhancing carrier separation and transfer. We also analyzed the influence of structural parameter on the absorptivity. The result indicates that the performance of our photodetector can be significantly improved by our design of the plasma structure, which provides a potential scheme for the application of plasma structure optoelectronic devices.

Introduction

Recently, graphene with high optical transparency, high electron mobility, and voltage-controlled conductivity has shown its unique application in photonic and optoelectronic devices such as tunable absorbers [1], high speed and broadband photodetectors [2], ultrafast lasers, touchscreens, OLEDs, and solar cells. As a direct-bandgap semiconductor, GaAs can collect and produce light more efficiently than indirect-bandgap silicon. Combining graphene and GaAs to form a heterojunction, the built-in electric field between graphene and GaAs can both suppress the dark current and promotes the separation of photogenerated carriers in the depletion region [3]. However, the interaction between graphene and incident light passing through it once is very weak because of its ultrathin structure so that monolayer.

graphene can only absorb 2.3% of the vertically incident light [4]. Hence, the photoresponsivity of pure graphene device is low and the maximum responsivity of graphene photodetector is below 10 mA/W [5]. How to enhance the interaction between the light field and graphene is crucial to improve the performance of graphene-based optoelectronic devices.

There are several methods to enhance light absorption in the visible and near-infrared wavelength ranges. In some research studies, the Fabry–Perot (F-P) cavity has been used to increase light absorption in graphene-based photodetectors [6, 7]. The photodetectors are integrated with an optical cavity, resulting in multiple reflections at resonance and enhanced absorption in graphene. Casalino et al. presented a vertically illuminated graphene-Si Schottky photodetectors enhanced by F-P cavity [8–10]. At 10 V reverse voltage, light is absorbed in graphene and the photocurrent can be generated with an improved external responsivity of 20 mA/W through the internal photon emission effect. Nematpour et al. simulated and fabricated an F-P resonator with single layer-graphene embedded at the cavity center [11]. With the interference of electromagnetic radiation,

✉ Lier Deng
  denglier@xatu.edu.cn

1 School of Opto-Electronic Engineering, Xi'an Technological University, Xi'an 710021, People's Republic of China

the experiment result shows that the absorption of single-layer graphene inside the cavity was 84% at 3150 nm with a bandwidth of 44 nm. The F-P cavity enhancement method is characterized by a small absorption band width, which makes it unsuitable for broad-spectrum photodetectors.

Under the action of incident electromagnetic field, the free electrons on the surface of the metal nanostructure oscillate collectively, then exciting surface plasmons. Recently, it has been revealed that plasmon resonance in metallic nanostructures can be used to increase the optical absorption by the near-field enhancement effect and high light trapping effect [12–15]. Recently, Yousif et al. presented and established a gold surface plasmon polariton (SPP) GaAs photodetector that achieves high internal quantum efficiency [16]. At a wavelength of 600 nm, the internal quantum efficiency with the SPP was 85%, an enhancement of 43%. The excellent performance is attributed to the subwavelength restraint of the optical power in a photoconductive-based gold SPP GaAs that enables high internal quantum efficiency. Moreover, the recombination of the SPP in the photodetector provides greater photocurrent and responsivity. Varasteanu et al. reported the plasmon-enhanced photoresponse of a novel photodetector architecture based on silicon nanoholes (SiNHs) following the incorporation of four different types of metallic nanowires (AgNWs, AuNWs, NiNWs, PtNWs) onto the silicon surface [17]. The self-powered AgNWs/SiNH device increased the photo-to-dark current ratio by two orders of magnitude, responsivity of 30 mA/W, and detectivity of 2×10^{11} Jones. Compared to the bare SiNH device, the AuNWs/SiNH device had significantly enhanced responsivity up to 15 mA/W, attributed mainly to the increased photo-induced carrier injection and high electric field distribution surrounding the nanowires.

Recently, Liang et al. presented a nanometer-sized metallic ellipse wall grating structures to improve light the transmission within the device [18]. Compared to slits with straight walls, the metal slits with nonlinearly tapered ellipse walls can collect more light on the upper surface, which is coupled into a gap plasmon polariton propagating along the ellipse walls, then delivers the light at the smaller exit slit opening. Therefore, we present a graphene/GaAs heterojunction photodetector based on ellipse wall grating-nanowire (EWG-NW) structure. Moreover, the graphene/GaAs photodetector is self-powered and does not require an additional power supply. We used Ag as the deposited metal film material because it has a lower dissipation rate in the visible region compared to other metals and it has well-defined plasma properties. Visible regions are considered in this paper that covers a wavelength range from 400 to 800 nm. Compared with graphene/GaAs photodetector based on plain structure, our devices exhibit a higher light absorption and responsivity at 0 bias voltage. Finite element method simulation suggests that the plasmonic EWG-NW structure can significantly enhance the absorption of the GaAs layer by optimizing the geometric parameters of the EWG-NW structure, so that the absorption capacity, external quantum efficiency, responsivity, and spectrum of the heterostructure have been improved. In addition, we investigate the influences of modification of structural parameters on detector performance.

Theory and Model Design

Figure 1 illustrates the schematics of graphene/GaAs photodetector based on EWG-NW structure. From top to bottom, there are the ellipse wall grating, the graphene layer, and the GaAs layer. Graphene can be used not only as transparent conductive layer, but also as a light-absorbing layer. The AgNWs are embedded in GaAs. The thicknesses of GaAs and bilayer graphene are 2 μm (t) and 1 nm, respectively. The unit period and separation between the two gratings are 0.3 μm (p) and 140 nm (b), respectively. The boundary of the ellipse walls can be mathematically described by $x^2/\delta^2 + y^2/h^2 = 1$, the semi-minor axis of the ellipse walls grating is 60 nm (δ), and semi-major axis (metal film thickness) is 120 nm (h). Each ellipse wall is a quarter of elliptic curve described by the above equation. This kind of grating is deposited on the substrate. This structure makes the slit opening decrease nonlinearly from top to bottom. The period, radius, and depth of the AgNWs are 0.3 μm (p), 20 nm (r), and 90 nm (d), respectively. The active area of the photodetector is 0.75 mm². We select AM1.5G (the standard spectrum of the Earth's surface) as the input power density.

The relevant photoresponse mechanism for graphene/GaAs heterostructure detector can be explained with the help of energy band diagram in Fig. 1c. Graphene is the p-type doping and its Femi level is 4.8 eV which is 0.33 eV below the Dirac point before illumination. The work function of n-type doping GaAs is 4.71 eV. Due to the difference of Fermi level, a portion of electrons in GaAs would move into the graphene and cause an upward bending of energy levels in GaAs near the interface; thus, a built-in electric field is formed which is directing from the GaAs to the graphene. Upon the illumination of light, the photocarriers generated in GaAs and graphene will be separated by the built-in electric field, thus giving rise to the photocurrent.

Doping of GaAs substrates can be achieved using metal organic chemical vapor deposition (MOCVD), and graphene can be grown under vacuum conditions using chemical vapor deposition (CVD). Nano-arrays of different shapes and sizes can be prepared on metal films using focused ion beam and electron beam etching techniques. The fabrication procedure for this structure is similar to the one implemented in Ref. [19]. The various design parameters of the heterojunction photodetectors required for simulation calculations are provided in Table 1.
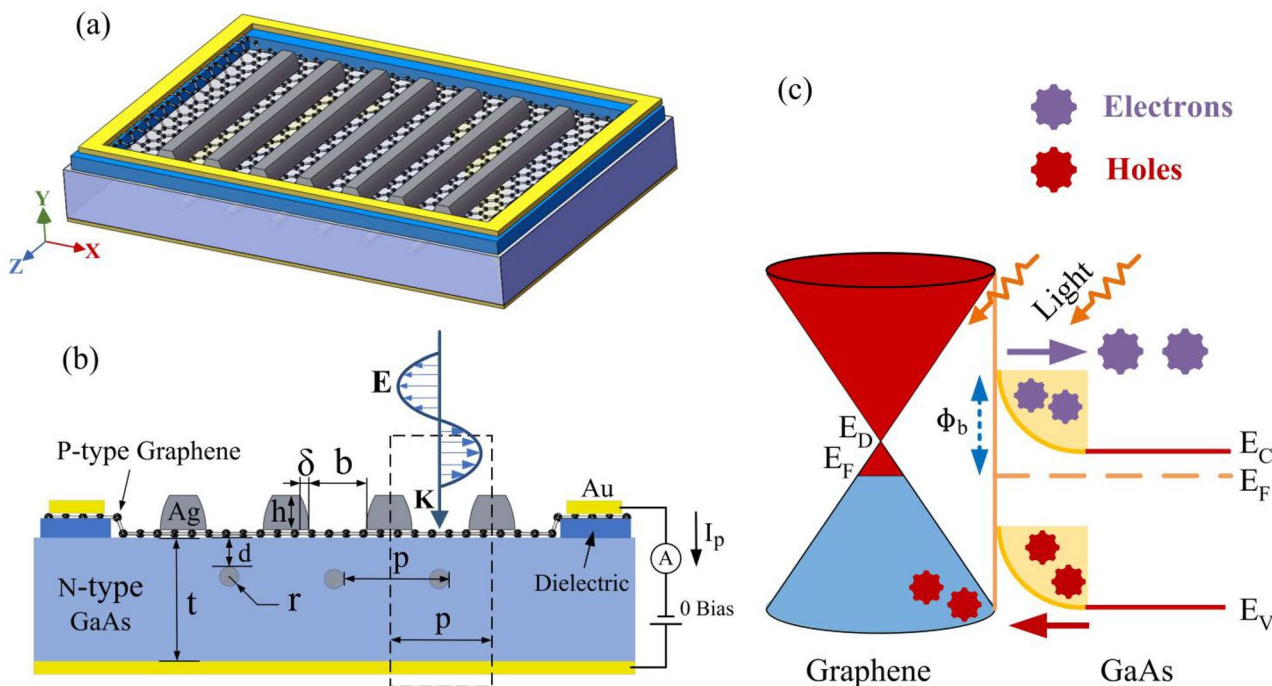
Fig. 1 **a** Schematic diagram of the designed photodetector with EWG-NW structure. **b** Cross section of the detector and simulation unit of the proposed structures. **c** Energy band diagram of graphene/GaAs heterojunction under zero bias illumination

In Fig. 1b, a periodic element in the dotted box is used to establish a two-dimensional finite element model. Periodic boundary conditions are used on both sides of the model to assume the structure in the x direction is infinite and the perfect matching layers make the simulation closer to the real situation. The incident light is perpendicular to the upper surface of the photodetector and the electric field component is parallel to x direction. The numerical method is used to solve the Maxwell equations to obtain the spatial distribution of the electromagnetic field.

Table 1 Parameters of the structure design of graphene/GaAs heterojunction photodetectors based on plasma

	P-graphene	N-GaAs	Ag
Refractiveindex	Ref. [20]	Ref. [21]	Ref. [22]
E_g[eV]	0.55	1.42	-
χ[eV]	4.80	4.07	-
N_c[1/cm^3]	1.00×10^{21}	9.19×10^{24}	-
N_v[1/cm^3]	1.04×10^{21}	4.07×10^{23}	-
μ_n[cm^2/(V·s)]	40,000	8000	-
μ_p[cm^2/(V·s)]	650	200	-
τ_n	5 [ps]	4 [ns]	-
τ_p	5 [ps]	10 [ns]	-
Doping[1/cm^3]	3.5×10^{16}	2.6×10^{16}	-

$$\nabla \times \mu_r^{-1} \times (\nabla \times \mathbf{E}) - k_0^2(\varepsilon_r - \frac{j\sigma}{\omega\varepsilon_0})\mathbf{E} = 0 \quad (1)$$

$$\nabla \times [(\varepsilon_r - \frac{j\sigma}{\omega\varepsilon_0})^{-1}\nabla \times \mathbf{H}] - k_0^2\mu_r\mathbf{H} = 0 \quad (2)$$

where k_0 is the wave vector; ω is the angular frequency of the incident light; ε_r and μ_r are the relative permittivity and relative permeability of the medium, respectively; ε_0 is the vacuum dielectric constant; $\mathbf{E}$ and $\mathbf{H}$ are electric and magnetic fields; σ is conductivity. The absorptivity of the semiconductor region can be calculated by the ratio of the total power dissipation density $w(x,y,z)$ in graphene and GaAs to the incoming power through the exposed surface area A by Eq. (3). And the power dissipation density $w(x,y,z)$ can be calculated by Eq. (4) [23, 24].

$$\alpha = \frac{\iiint w(x, y, z)dV}{\frac{1}{2}c_0\varepsilon_0|\mathbf{E}_{inc}|^2 A\cos\theta} \quad (3)$$

$$w(x, y, z) = \frac{1}{2}\varepsilon_0\omega\varepsilon^\varepsilon(x, y, z)|\mathbf{E}(x, y, z)|^2 \quad (4)$$

After the light irradiates on the photodetector and is absorbed, photons with enough energy can excite electrons from the covalent bond to produce photogenerated carriers. Before recombination, these photogenerated

charge carriers will be pulled apart by an internal electric field, causing electrons to drift toward the N region and holes to drift toward the P region, forming a current. The process of photoelectric conversion can be described by the steady-state carrier transport equation and Poisson equation.

$$\nabla\left[-D_n\nabla n + n\mu_n\left(\nabla\Phi + \frac{\nabla\chi}{q} + \frac{K_BT}{q}\nabla\ln N_c\right)\right] = G - U \tag{5}$$

$$\nabla\left[-D_p\nabla p + p\mu_p\left(\nabla\Phi + \frac{\nabla\chi}{q} + \frac{\nabla E_g}{q} - \frac{K_BT}{q}\nabla\ln N_v\right)\right] = G - U \tag{6}$$

$$\nabla^2\Phi = \frac{q}{\varepsilon_0\varepsilon_r}(n - p - N_D + N_A) \tag{7}$$

where D_n and D_p are are the diffusion coefficients, n and p are concentrations, μ_n and μ_p represent the mobilities for electron and hole, N_c and N_v are the effective conduction and valence band density of states, respectively, $\Phi\Phi$ is the electrostatic potential, χ is the electron affinity, K_B is the Boltzmann constant, q is the electron charge, E_g is the band gap, T is the temperature, ε_r is the relative permittivity, N_D and N_A are the donor and acceptor concentrations, respectively, $G(x,y,z)$ is the carrier generation distribution.

Several key performance parameters are needed to evaluate a photodetector performance. Usually, the responsivity (R), current density (J), external quantum efficiency (EQE),

and detectivity (D^*) can be further analyzed, which are, respectively, defined as

$$R = \frac{I_{light} - I_{dark}}{P_{in}A} = \frac{I_{ph}}{P_{in}A} \tag{8}$$

$$\text{EQE} = \frac{Rhc}{q} \tag{9}$$

$$D^* = \frac{R}{\sqrt{2qJ_{dark}}} \tag{10}$$

where I_{light}, I_{dark}, P_{in}, A, c, q, h, and J_{dark} are the output current in the presence of light, dark current, power density of input light, effective light area of the device, light speed, electron charge, Planck's constant, and dark current density, respectively.

Results and Discussion

As Fig. 2 shows, we simulate the absorption spectrum of semiconductor materials in the heterojunction photodetectors for the plain, metal nanowires, ellipse walls grating, and EWG-NW structures. The incident wave is TM and the wavelength is between 400 and 800 nm. The absorption of the plain graphene/GaAs heterojunction photodetector rises slowly from 39.9% and stabilizes around 50%. With the

Fig. 2 Absorption spectra of graphene/GaAs heterojunction photodetectors based on plain structure, nanowire structure, ellipse wall grating structure, and EWG-NWs structure
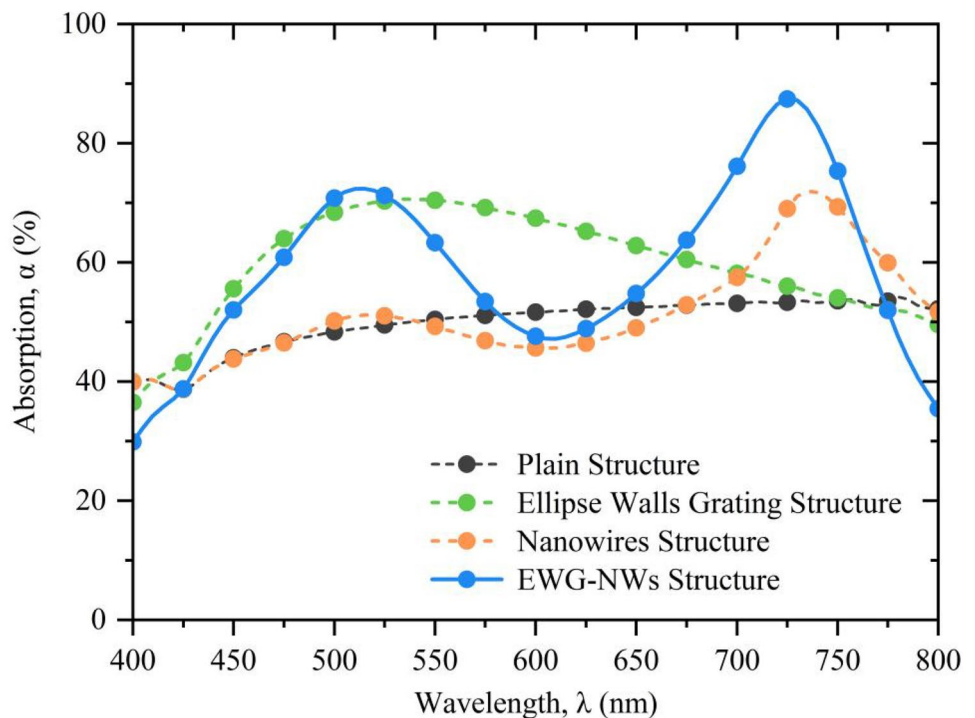
introduction of metal ellipse wall gratings and nanowires, the excitation of the plasma leads to increasing absorption capacity of photodetectors, and the metallic nanostructures scatter the incident light, increase its effective propagation path length in the substrate, and improve the light absorption of the semiconductor material. The highest absorptivity was 70.6% at 540 nm for ellipse wall grating structure with a plasmon mode and the highest absorptivity was 71.7% at 740 nm for nanowire structure. Compared with the other three structures, our proposed EWG-NW structure shows double resonance absorption peaks at 510 nm and 725 nm with peak absorptivities of 72.3% and 87.4%, respectively. In addition, the positions of the first and second peaks basically coincide with the positions of the absorption peaks of the elliptical wall and nanowire structures. The graphene film is particularly thin, so it is difficult for it to achieve high absorption independently. However, the designed EWG-NW plasmonic structure can excite magnetic polaritons (MP) and localized surface polaritons (LSP) mode, resulting in a local enhanced coupling effect of incident light. The local enhanced coupling effect enhances the absorption of light by semiconductor materials with photoelectric conversion properties, thus further improving the electrical signal response.

To gain an insight of mechanism that causes enhanced absorption of the EWG-NW structure, thus contributing the photocurrent, the electromagnetic field distributions were calculated at a resonant wavelength of 510 nm and 725 nm. These two bands represent the strongest absorption of plasmonic structure. The simulation results are presented in Fig. 3. As shown in Fig. 3a, the enhanced magnetic field is confined to the bottom of the grating and within the semiconductor region, indicating that there is a larger energy confinement at the metal surface, but the intensity is

not as strong as the enhancement at the surface of AgNWs. The electric field vector moves along the position of the enhanced magnetic field, forming a closed loop around the notch. This excitation pattern is caused by MP resonance. The MP resonance is a strong coupling between the magnetic resonance inside the structure and the external electromagnetic waves to achieve a strong magnetic resonance effect. Figure 3b shows that the magnetic field enhancement mainly occurs on the top surface of AgNWs, and the location of the electromagnetic field enhancement is more favorable for the absorption and photovoltaic conversion of the semiconductor materials. The results indicate that the excitation of LSP mode can improve the absorption capacity of semiconductor materials. LSP refers to the mutual coupling of electromagnetic waves with free electrons in metals whose dimensions are much smaller than the wavelength of the waves. This indicates that the coupling of LSP and MP enhances the absorption of the structure. At the wavelength of 510 nm MP enhancement dominates the absorption enhancement of the semiconductor, while as the wavelength increases to 725 nm, the absorption enhancement is mainly from LSP.

The above analysis shows that the EWG-NW structure can improve the photoelectric conversion efficiency of photodetector semiconductor materials by exciting surface plasmon excitations. Therefore, we analyzed the effect of structural parameters on the absorption spectra of the semiconductor material of the photodetector. As shown in Fig. 4a, the first absorption peak gradually disappears when the period is greater than 0.35 μm. As the period increases, the second peak position red-shifts and the bandwidth increases and then decreases. Figure 4b shows that the position of the first peak is significantly red-shifted as the
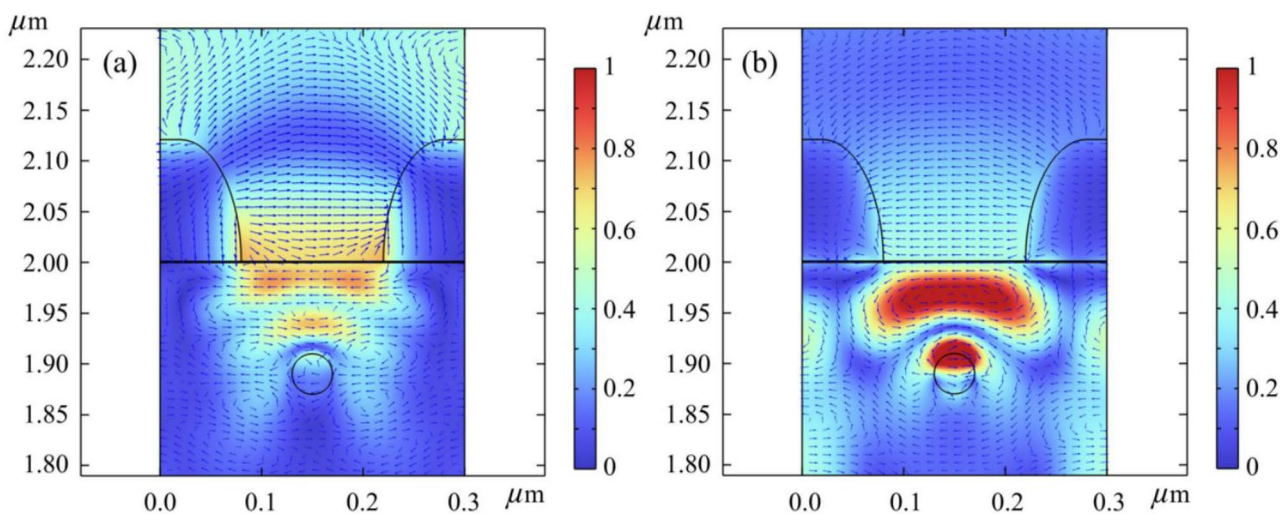

Fig. 3 Normalized electromagnetic field distribution, the contours, and the blue arrows represent the magnetic field and electronic field, respectively. **a** λ = 510 nm. **b** λ = 725 nm
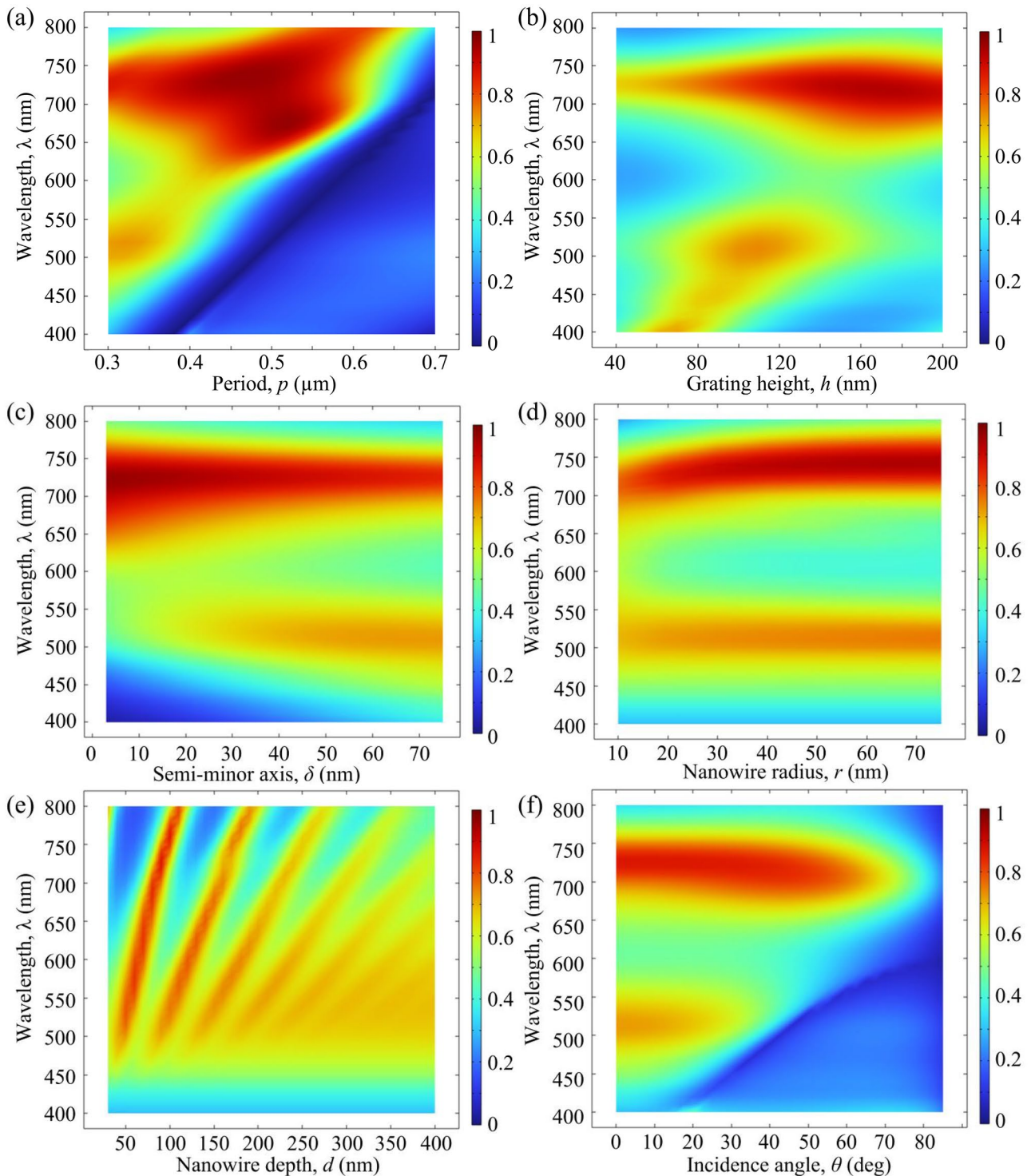
Fig. 4 Absorptivity contours for various geometric parameters, **a** Period. **b** Grating height. **c** Semi-minor axis. **d** Nanowire radius. **e** Nanowire depth. **f** Incidence angle

grating height increases and gradually disappears when the height is greater than 120 nm. The intensity of the second absorption peak gradually increases and the bandwidth first increases and then decreases. As shown in Fig. 4c, the first

absorption peak appears when the semi-minor axis is greater than 30 nm, and as the semi-minor axis increases, the first peak position is slightly blue-shifted. However, the bandwidth of the second peak gradually decreases. Compared to

the nonlinear elliptical-walled metallic gratings ($\delta = 60$ nm), photodetectors based on straight-walled metallic grating structure ($\delta = 0$ nm) have higher absorptivity at the long wavelengths but lower absorptivity at the short wavelengths. This suggests that the larger slit opening of the nonlinear elliptical-walled metal grating results in smaller reflections on the top surface of the grating. The small reflection may allow most of the energy to flow into the elliptical slit and couple with the plasmonic excitations excited by the metal nanowire structure into the graphene/GaAs region. As Fig. 4d shows, as the radius of the nanowire increases, the first peak intensity increases slightly, but the intensity of the absorption between the two peaks decreases. The position of the second absorption peak red-shifted when the nanowire radius is increased from 10 to 20 nm, and the peak position remains essentially unchanged when the radius is greater than 20 nm. As shown in Fig. 4e, the absorption peaks significantly red-shifted with the increase of nanowire depth, and the absorption peaks gradually disappear when the depth is greater than 300 nm. Based on the above analysis, it is

observed that the absorption peak intensity and position can be efficiently controlled through the period, grating height, semi-minor axis, and nanowire depth. We comprehensively consider the absorptivity from 400 to 800 nm, and when the grating period, height, semi-minor axis, and the radius and depth of the silver nanowires are 0.3 µm (p), 120 nm (h), 60 nm (δ), 20 nm (r), and 90 nm (d), respectively, our design structure can obtain high absorptivity in the visible region, which indicates that it is suitable as an optoelectronic device in the visible light region. As shown in Fig. 4e, there are two obvious absorption peaks when the incidence angle is less than 30°. The first peak disappears when the angle of incidence is greater than 30°, while the second peak gradually disappears when the angle of incidence is greater than 70°, which indicates that the second peak has a better angular insensitivity compared to the first peak. According to the above analysis we can optimize the structural parameters for higher absorptivity in the visible range.

In addition to the optical characteristics, in order to better evaluate the performance of our proposed graphene/GaAs
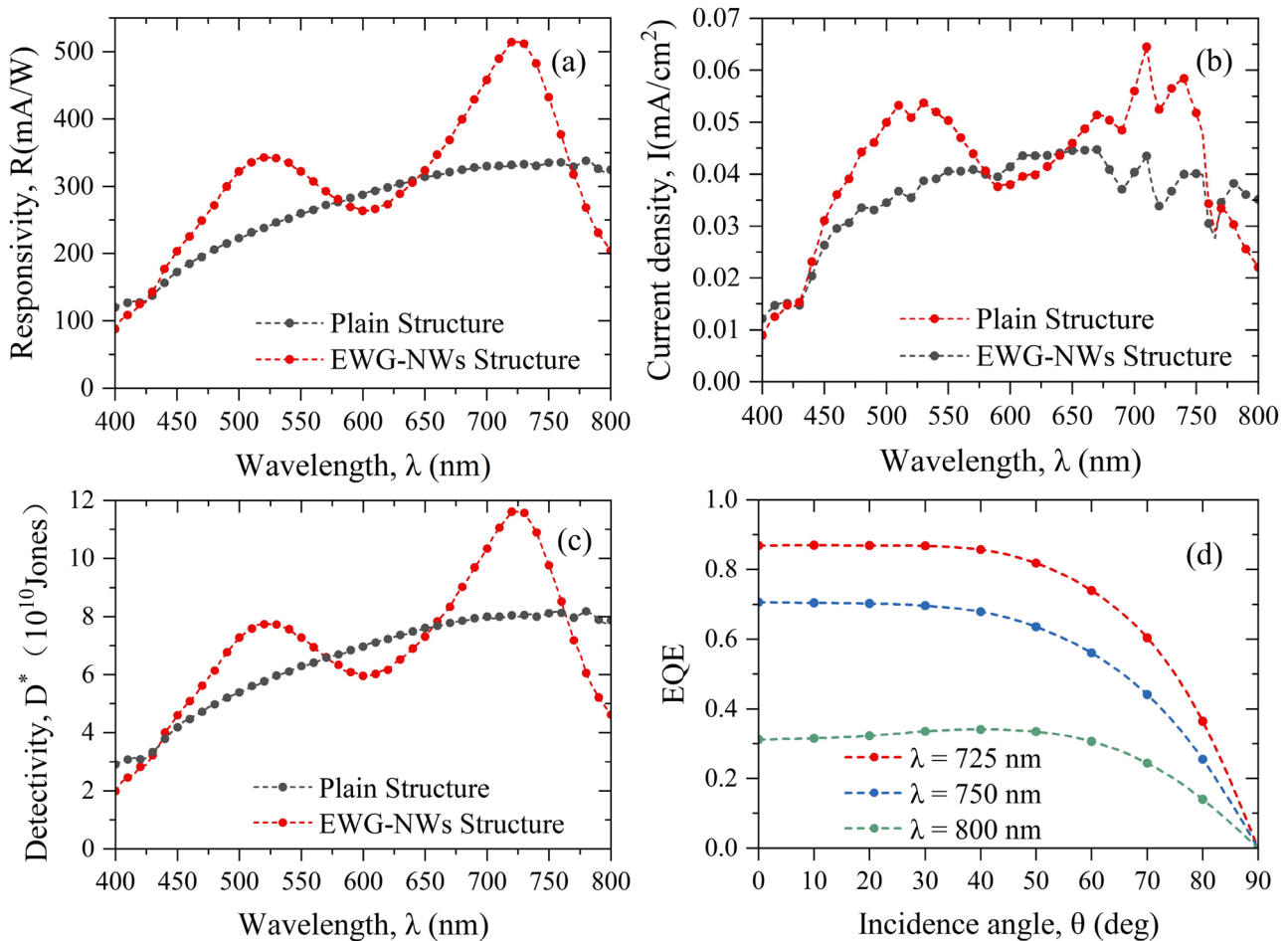

Fig. 5 Electrical characteristics of photodetectors based on plain structure and EWG-NWs structure at 0 bias voltage. **a** Responsivity of photodetectors. **b** Current density of photodetectors. **c** Detectivity of photodetectors. **d** EQE of photodetectors in different wavelength

Table 2 Performance comparison with other plasma-enhanced photodetectors

Device structures	Wavelength (nm)	R (mA/W)	D* (Jones)	Ref
Ag ellipse walls grating/AgNWs/graphene/GaAs	725	514	1.16×10^{11}	Present work
Ag ellipse walls grating/AgNWs/graphene/GaAs	520	343	7.74×10^{10}	Present work
AgNPs/graphene/GaAs	633	142	2.02×10^{13}	[3]
Au-SiO$_2$ grating/graphene/SiO$_2$/Si	550	200	-	[25]
AgNPs/SiO$_2$/Si	514	2.2	-	[26]
AuNPs/graphene/AgNPs/graphene/SiO$_2$/Si	450	340	5×10^7	[27]
AgNWs/SiNHs	365	30	2×10^{11}	[17]

heterojunction photodetector based on the EWG-NW structure, some main electrical characteristics at zero bias voltage are also calculated, as shown in Fig. 5. When photons are incident into the heterostructure, they excite photogenerated carriers and generate current in the presence of the built-in electric field of the heterostructure. And the plasma resonance excited by metallic nanostructures can increase the carrier concentration in semiconductors. Figure 5a shows the distribution curve of responsivity with spectrum. It is evident that the responsivity increases with the light absorption capacity. The maximum responsivity of our proposed structure at 725 nm is 514 mA/W, which is significantly higher than that of the grating-less structure at the same wavelength position (330 mA/W). Figure 5b shows that the current density of the EWG-NW structure is higher than that of the plain graphene/GaAs structure in the range of 430–580 nm and 640–770 nm. This indicates that plasma can increase the current density in specific regions. At 710 nm, the maximum current density of the excited plasma structure is 0.064 mA/cm^2. At the same wavelength, the current density of the normal structure is 0.043 mA/cm^2, while it increases by 0.021 mA/cm^2 at 710 nm. As shown in Fig. 5c, the enhancement of detectivity is also positively correlated with the absorption intensity. The maximum detectivity for the EWG-NW structure and the plain structure are 1.16×10^{11} Jones and 8.17×10^{10} Jones, respectively. In order to analyze the incident angle dependence of the EQE, the variation of the EQE with different incident angles at different incident wavelengths is calculated. The maximum EQE of the EWG-NW structure is 0.869 at 725 nm as shown in Fig. 5d. Meanwhile, it can be found that the EQE remains basically unchanged for different wavelengths when the angle of incidence is less than 40° and then decreases gradually with the increase of the incident angles. From Table 2, it can be clearly seen that the device responsivity is better than the other devices reported in the literature when simulated under the standard solar spectrum.

Conclusion

In conclusion, we designed and simulated a graphene/GaAs heterojunction photodetector based on EWG-NW structure. Due to the plasma-enhanced light-matter interactions, the absorptivity and electrical characteristics of the devices are enhanced, which are significantly better than those of ordinary graphene/GaAs photodetectors. Simulation results show a significant improvement in the responsivity in the wavelength range of 400 nm to 800 nm. At zero bias voltage, the device achieves a responsivity of up to 514 mA/W at 725 nm, which corresponds to current density of 0.064 mA/cm^2, detectivity of 1.16×10^{11}, and EQE of 86.9%. The results of present work demonstrate the great potential of photodetectors based on EWG-NW structures as self-powered broadband heterojunction photodetectors.

Declarations

Ethics Approval Not applicable.

Consent to Participate Not applicable.

Consent for Publication Not applicable.

Competing Interests The authors declare no competing interests.

References

1. Pourmand M, Choudhury PK, Mohamed MA (2021) Tunable absorber embedded with GST mediums and trilayer graphene strip microheaters. Sci Rep 11:3603
2. De Nicola F, Puthiya Purayil NS et al (2020) Graphene plasmonic fractal metamate-rials for broadband photodetectors. Sci Rep 10:6882
3. Lu Y, Feng S, Wu Z et al (2018) Broadband surface plasmon resonance enhanced self-powered graphene/GaAs photodetector with ultrahigh detectivity. Nano Energy 47:140–149
4. Yan Z, Gao L, Tang C, Lv B, Gu P, Chen J, Zhu M (2022) Simultaneously achieving narrowband and broadband light

absorption enhancement in monolayer graphene. Diam Relat Mater 126:109122

5. Zhang BY, Liu T, Meng B, Li X, Liang G, Hu X, Wang QJ (2013) Broadband high photoresponse from pure monolayer graphene photodetector. Nat Commun 4:1811

6. Yuan Z, Wu PC, Chen YC (2022) Optical resonator enhanced photovoltaics and photocatalysis: fundamental and recent progress. Laser Photonics Rev 16:2100202

7. Jafari B, Gholizadeh E, Golmohammadi S, Ebadzadeh M, Soofi H, Aghili S (2023) An innovative method for adjustable broadband THz to mid-IR optical modulator using graphene gratings surface plasmon Fabry-Perot resonances with low insertion loss, high speed and modulation depth. Opt Commun 530:129200

8. Casalino M et al (2017) Vertically illuminated, resonant cavity enhanced, graphene-silicon Schottky photodetectors. ACS Nano 11:10955–10963

9. Casalino M (2018) Design of resonant cavity-enhanced Schottky graphene/silicon photodetectors at 1550 nm. J Lightwave Technol 36:1766–1774

10. Casalino M, Sirleto L, Moretti L et al (2009) Back-illuminated silicon resonant cavity-enhanced photodetector at 1550 nm. Phys E 41:1097–1101

11. Nematpour A, Lisi N, Lancellotti L, Chierchia R, Grilli ML (2021) Experimental mid-infrared absorption (84%) of single-layer graphene in a reflective asymmetric Fabry- Perot filter: implications for photodetectors. ACS Appl Nano Mater 4:1495–1502

12. Huang JA, Luo LB (2018) Low-dimensional plasmonic photodetectors: recent progress and future opportunities. Adv Opt Mater 6:1701282

13. Hekmat M, Shafiekhani A, Khabir M (2022) Near field and far field plasmonic enhancements with bilayers of different dimensions AgNPs@ DLC for improved current density in silicon solar. Sci Rep 12:19663

14. Talebi H, Emami F (2022) Design of ultrathin hole-transport-layer-free perovskite solar cell with near-infrared absorption enhancement using Ag NPs. Opt Commun 520:128553

15. Echtermeyer TJ, Milana S, Sassi U, Eiden A, Wu M, Lidorikis E, Ferrari AC (2016) Surface plasmon polariton graphene photodetectors. Nano Lett 16:8–20

16. Yousif B, Abo-Elsoud MEA, Marouf H (2020) High- performance enhancement of a GaAs photodetector using a plasmonic grating. Plasmonics 15:1377–1387

17. Alqanoo AA, Ahmed NM, Hashim MR, Almessiere MA, Taya SA, Zyoud SH (2022) Silver nanowires assisted porous silicon for high photodetector sensitivity using surface plasmonic phenomena. Sens Actuators A 347:113942

18. Liang Y, Peng W, Hu R, Zou H (2013) Extraordinary optical transmission based on subwavelength metallic grating with ellipse walls. Opt Express 21:6139–6152

19. Ai B, Yu Y, Möhwald H, Zhang G, Yang B (2014) Plasmonic films based on colloidal lithography. Adv Coll Interface Sci 206:5–16

20. El-Sayed MA et al (2021) Optical constants of chemical vapor deposited graphene for photonic applications. Nanomaterials 11:1230

21. Papatryfonos K et al (2021) Refractive indices of MBE- grown $Al_xGa_{(1-x)}As$ ternary alloys in the transparent wavelength region. AIP Adv 11:025327

22. Ferrera M, Magnozzi M et al (2019) Temperature-dependent permittivity of silver and implications for thermoplasmonics. Phys Rev Mater 3:105201

23. Pan Q, Guo Y, Zhou S, Shuai Y, Tan H (2020) Analysis of infrared spectroscopy absorption characteristics of graphene transferred to grating structures. J Quant Spectrosc Radiat Transfer 254:107185

24. Pan Q, Zhou S, Guo Y et al (2022) Enhanced photoelectric responsivity of bilayer graphene/GaAs photodetector using plasmon resonance grating structures. Optik 259:169031

25. Li J, Zhao C et al (2019) Metamaterial grating-integrated graphene photodetector with broadband high responsivity. Appl Surf Sci 473:633–640

26. Liu Y, Cheng R, Liao L, Zhou H, Bai J, Liu G, Liu L, Huang Y, Duan X (2011) Plasmon resonance enhanced multicolour photodetection by graphene. Nat Commun 2:579

27. Suo H, Yang S, Ji P, Wang Y (2021) Multi-band enhanced graphene photodetector based on localized surface plasmon. Sens Actuators A 322:112627